Monitoring and Prevention Strategies for Iron and Aluminum Pollutants in Acid Mine Drainage (AMD): Evidence from Xiaomixi Stream in Qinling Mountains

Xiaoya Wang [1], Min Yang [1,2,*], Huaqing Chen [2,3], Zongming Cai [1], Weishun Fu [1], Xin Zhang [2], Fangqiang Sun [3] and Yangquan Li [4]

[1] School of Resources Engineering, Xi'an University of Architecture and Technology, Xi'an 710055, China; xiaoya723@xauat.edu.cn (X.W.); czm@xauat.edu.cn (Z.C.); fuweishun2022@xauat.edu.cn (W.F.)
[2] Field Observation Base for Environmental Geology of Typical Mines in Shaanxi Province, Ministry of Natural Resources, Xi'an 710054, China; chuaqing@mail.cgs.gov.cn (H.C.); zhangxin17@xauat.edu.cn (X.Z.)
[3] Xi'an Geological Survey Center of China Geological Survey, Xi'an 710054, China; sfangqiang@mail.cgs.gov.cn
[4] Xi'an Baling Space Information Technology Co., Ltd., Xi'an 710054, China; 18991328601@163.com
[*] Correspondence: ymin@xauat.edu.cn

Abstract: Acid mine drainage (AMD) generated during the exploitation and utilization of mineral resources poses a severe environmental problem globally within the mining industry. The Xiaomixi Stream in Ziyang County, Shaanxi Province, is a primary tributary of the Han River, which is surrounded by historically concentrated mining areas for stone coal and vanadium ores. Rainwater erosion of abandoned mine tunnels and waste rock piles has led to the leaching of acidic substances and heavy metals, which then enter the Haoping River and its tributaries through surface runoff. This results in acidic water, posing a significant threat to the water quality of the South-to-North Water Diversion Middle Route within the Han River basin. According to this study's investigation, Xiaomixi's acidic water exhibits yellow and white precipitates upstream and downstream of the river, respectively. These precipitates stem from the oxidation of iron-bearing minerals and aluminum-bearing minerals. The precipitation process is controlled by factors such as the pH and temperature, exhibiting seasonal variations. Taking the Xiaomixi Stream in Ziyang County, Shaanxi Province, as the study area, this paper conducts field investigations, systematic sampling of water bodies and river sediments, testing for iron and aluminum pollutants in water, and micro-area observations using field emission scanning electron microscopy (FESEM) on sediments, along with analyzing the iron and aluminum content. The deposition is analyzed using handheld X-ray fluorescence (XRF) analyzers, X-ray diffraction (XRD), and visible–near-infrared spectroscopy data, and a geochemical model is established using PHREEQC software. This paper summarizes the migration and transformation mechanisms of iron and aluminum pollutants in acidic water and proposes appropriate prevention and control measures.

Keywords: acid mine drainage; mine environmental pollution; sample testing

1. Introduction

With the continuous development of the socio-economy, the exploitation and utilization of mineral resources have become an indispensable part of human life. Inevitably, some pollution is generated during the process of mineral resource development, and acid mine drainage (AMD) is one of the major challenges faced by the global mining industry [1]. AMD is mainly generated by the oxidation of sulfide minerals exposed to air, water,

and microbial activity. The main sources include ore and rock waste dumps, open-pit mining, tailings ponds, underground mines, and acidic soils [2]. AMD is strongly acidic, with a pH value generally below 4 [3], and contains high concentrations of heavy metal ions and sulfates. The discharge of untreated AMD poses a risk of contaminating nearby water sources, as well as flora and fauna, not only adversely affecting biodiversity but also causing soil acidification that can reach the top of the food chain, posing a hazard to human health [4]. The discharge of untreated acidic water can contaminate groundwater, disrupt aquatic ecosystems, and alter the granular structure of soil, leading to soil hardening and salinization [5]. Several reasons can lead to the formation of acidic wastewater in mines. The major reasons are the following. (1) During the mining process, large amounts of groundwater infiltrate into the mining face, and when this mine water is discharged to the surface, it becomes the primary source of acidic wastewater [6]. (2) In the ore-processing process, the use of beneficiation processes that involve the addition of acidic reagents results in the discharge of wastewater that is a significant source of acidic wastewater and harmful substances [7]. (3) The large amounts of waste rock and tailings containing sulfide minerals discharged during mine production, when piled up in the open air, continuously come into contact with air, water, or water vapor, generating metal ions and sulfate ions. When exposed to rainwater or piled near rivers and lakes, the resulting acidic water can rapidly spread over a large area [8]. Due to its large volume, long formation time span, and dispersed origins, AMD has become one of the most challenging issues in mine environmental remediation [9–16]. No signs of the survival of fish, aquatic plants, or plankton have been found in the rivers within the study area due to the impact of acidic water.

The Xiaomixi Stream basin in the survey area is rich in stone coal resources and has always been the main production area for stone coal in the Qinling Mountains, providing an important source of fuel for regional economic development and people's lives. Since the 1950s, large-scale mining activities were carried out during the iron- and steel-smelting campaigns, and the construction of the Xiangyu Railway and the 310 Provincial Highway, without any preventive measures being taken, leaving behind a large number of abandoned mines and slags [17,18]. The mining waste was piled up locally on the slopes situated near the tunnel entrances, on adjacent slopes of open-pit mines, and even in areas left by unauthorized mining. Rainwater erosion has led to acidic substances and heavy metals leaching out of rocks into the Haoping River and its tributaries (through surface runoff processes), affecting water quality and forming acidic "yellow precipitate" and "white precipitate". The iron in the acidic water mainly comes from the oxidation of pyrite [19]; the aluminum comes from the dissolution of aluminum-bearing minerals (such as Al_2O_3 and aluminum clay) in symbiotic or associated environments, which consume H^+ during dissolution, resulting in increased concentrations of Al ions and pH values, promoting the hydrolysis of iron and aluminum and the precipitation of secondary minerals such as jarosite, schwertmannite, and alunite [20]. The current state of mine pollution is depicted in Figure 1, showing both yellow (a) and white (b) precipitates. In December 2021, the Third Central Ecological and Environmental Protection Inspection Team inspected Shaanxi Province and found that the risk of environmental pollution caused by acidic mine water in the Haoping River Basin in Ziyang County was prominent. The Xiaomixi Stream, a first-order tributary of the Han River, poses a serious threat to the water quality and safety of the Middle Route of the South-to-North Water Diversion Project in the Han River Basin [21]. Acid mine drainage (AMD) is generated during the extraction and utilization of mineral resources. AMD contains high concentrations of cations such as Fe^{3+}, Fe^{2+}, Mn^{2+}, and Al^{3+}, as well as anions like SO_4^{2-}, and also includes toxic elements such as copper (Cu), mercury (Hg), lead (Pb), zinc (Zn), and arsenic (As), significantly degrading the water quality in the area [22]. The mass concentrations of these toxic element ions in water range

from a few milligrams to hundreds of milligrams per liter, and in some regions, they even exceed thousands of milligrams per liter, severely contaminating water, soil, and air, and causing illnesses through the food chain. It is no exaggeration to say that the deterioration of environmental quality poses a threat to human survival [23]. The removal of toxic elements from the environment is a crucial scientific and practical task [24]. To predict and control pollution and implement purification procedures, it is essential to identify the primary hydrogeochemical mechanisms controlling the transport of contaminants [25].

(**a**)   (**b**)

Figure 1. Current status of mining operations and surface water pollution in the study area: (**a**) yellow precipitate upstream; and (**b**) white precipitate downstream.

The objective of this study is to conduct laboratory tests on the characteristics of the Fe and Al ions in the surface water, the microscopic morphology of the sediments, and the relative content of Fe and Al ions through systematic field sampling. The characteristics of the Fe and Al ions in the surface water are determined using spectrophotometry to identify significant patterns in the variation of Fe and Al ions in acidic water along the river's hydrological pathway. The micro-morphology of the sediments and the relative content of iron (Fe) and aluminum (Al) ions are tested using field emission scanning electron microscopy (FESEM). Additionally, the sediments are analyzed using handheld X-ray XRF analyzers, X-ray diffraction (XRD), and visible–near-infrared spectroscopy data. For further testing, a geochemical model is established using PHREEQC software. These analyses aim to uncover the migration and transformation mechanisms of Fe and Al ions in surface water contaminated by acid mine drainage. Corresponding remediation measures are also proposed.

2. Materials and Methods

2.1. Study Area

Ankang is divided into two major regions by the Han River, with the Qinling Mountains to the north and the Daba Mountains to the south. The Han River, along with the Chi and Yue Rivers, marks the boundary between the Qinling Mountains and the Daba Mountains. The landform is characterized by high mountains on both the north and south sides, with river valleys and basins in the center. The survey area has a north subtropical humid monsoon climate [26]. To the north, the Qinling Mountains and their branch, Fenghuang Mountain, block the cold currents from the northwest, while to the south, the Renhe River serves as a natural water vapor channel, transporting warm and humid airflows from the southwest. As a result, the area enjoys abundant rainfall and a moderate climate, with no extreme heat in summer and no severe cold in winter. The climate is characterized by cold and rainy winters, rainy and droughty summers, warm and dry springs, and cool, wet, and rainy autumns. Rainfall is concentrated from June to September each year, with the highest amount in July. Ankang City is responsible for 66% of the water supply for the South-to-North Water Diversion Project [27]. In general, the annual precipitation decreases from southwest to northeast. In the past decade, precipitation has been mainly concentrated in summer, while it has been relatively scarce in spring, autumn, and winter, resulting in a climate characterized by more floods in summer and droughts in spring, autumn, and winter.

The geological structure of the working area is a complex syncline with relatively developed faults [28]. The main stratigraphic units within the area include the Banjiuguan Group $(O_3\text{-}S_1)b$ of the Late Ordovician to Early Silurian, which represents a suite of carbonaceous (siliceous) muddy clastic sedimentary rocks deposited in a sub-deep-sea basin environment. The lithology is dominated by black carbonaceous slate and carbonaceous siliceous rocks, with trachytic rocks intercalated in the middle to upper parts. The Jianzhuba Group $(\in j)$ of the Cambrian comprises gray and dark gray thin-bedded limestone and banded limestone, with minor amounts of marlstone and carbonaceous slate (phyllite) [29]. The Lujiaping Group $(\in_1 l)$ of the Cambrian is mainly composed of black slate, with intercalations of black thin-bedded siliceous rocks and minor limestone, siltstone, etc. Locally, it contains pyrite, siderite, phosphate nodules, and barite ore beds. It is in conformable contact with the Jianzhuba Group above. The Donghe Group (Od) of the Ordovician is conformably overlying the Jianzhuba Group and is in parallel unconformable contact with the Banjiuguan Group below.

A geographical location map and substrate map of the Xiaomixi Stream are shown in Figure 2. The Xiaomixi Stream is part of Donghe Town, located in the eastern region of Ziyang County. Donghe Town lies at the confluence of the Han, Donghe, and Ruhe Rivers. The Xiangyu Railway also passes through the town. Donghe Town is situated in the north subtropical humid monsoon climate zone, featuring a mild climate without severe cold in winter or extreme heat in summer. The Han River boasts a navigable distance of over 100 km within the town's territory, stretching from Ziyang upstream to Lan'gui and Ankang downstream. The Lanzi Highway, Dongda Highway, Chenghui Highway, and Gunsan Highway intersect each other, making the water and land transportation highly developed. The communication network coverage reaches 99%. The town is abundant in water, forest, grass, mineral, and tourism resources, including high-quality mineral resources such as coal, iron, copper, manganese, nickel, and quartz. Wheat, rice, corn, potatoes, and sweet potatoes are the main crops for grain production. The agricultural industries are dominated by sericulture, tea, citrus, vegetables, and livestock farming [30].

The Xiaomixi Stream basin in Ankang City is a first-order tributary of the Han River. Surrounded by areas where stone coal and vanadium mines were intensively mined in the

past, the acidic water generated from some abandoned mine tunnels and waste rock dumps has severely polluted the river water in the valley. The Xiaomixi Stream originates in Mixiliang in Gaoping Town and flows through Qiaoergou, Yunfeng Village, and Yuanjiayuanzi before converging into the Han River 2 km downstream from Dacao Village. The total length of the basin is 7.91 km, with a drainage area of 9.37 km^2, while the flow velocity of the river is 0.16 m per second, making it a small first-order tributary of the Han River. The basin has numerous mines spread widely, posing significant challenges for remediation and requiring substantial financial resources. According to preliminary investigations, there are 330 mine tunnels and 95 waste dumps in the river basin, with 280 mine tunnels and 55 waste dumps located within Ziyang County's jurisdiction. The waste dumps occupy an area of 308,200 square meters and have a volume of 2,459,800 cubic meters [21]. Most of these mines are ownerless, with the responsible entities no longer in existence.
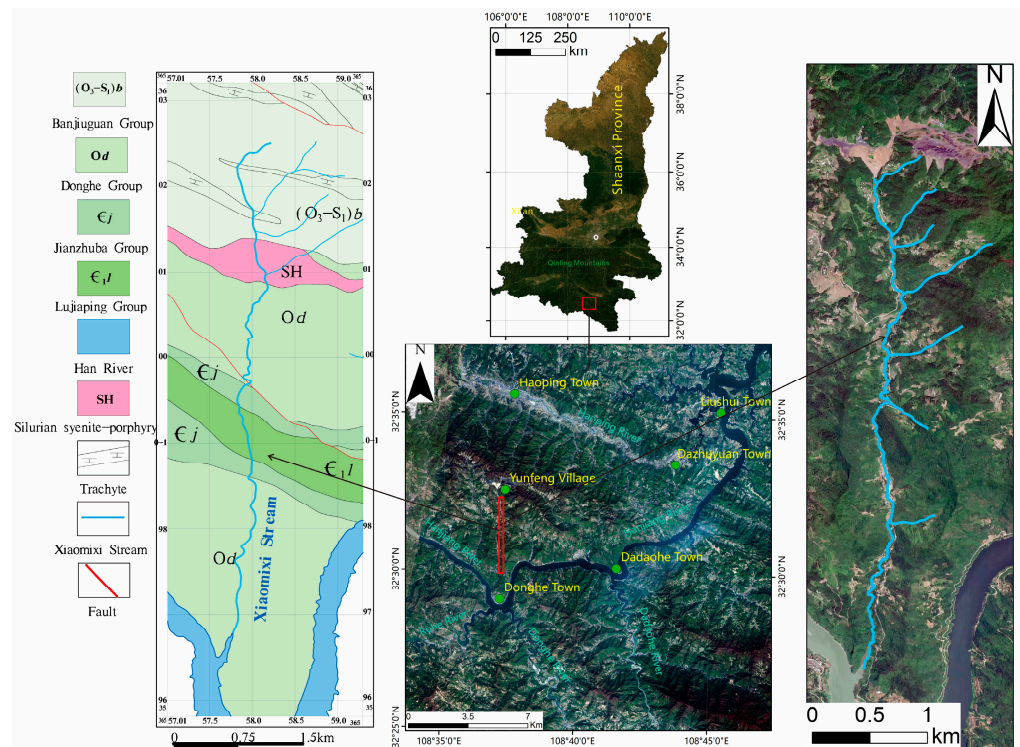

Figure 2. A geographical location map and substrate map of Xiaomixi.

2.2. Data Collection and Processing

The samples for this study were collected from the Xiaomixi Stream basin in Ankang City, Shaanxi Province, following the strict procedures outlined in the "Technical Specifications for Monitoring the Quality of Surface Water Environment" (HJ91.2-2022).

Information collection was conducted on the surrounding environment of the exploration area, and sampling points were appropriately set up. The purpose of water sample collection is to obtain test indicators that can represent high, medium, and low results. To achieve this, samples need to be collected from different reaches of the river. The principle when sampling is to ensure that the sample points are evenly distributed, with each sampling point being placed at an average distance along the entire length of the river. The distribution of the sampling points is shown in Figure 3.

A total of 13 surface water samples and 13 river sediment samples were collected from the Xiaomixi Stream basin. The weather was fine on the day of the sample collection, and the water quality was minimally affected by the temperature. The on-site collection and testing process is shown in Figure 4. The collected sediments are shown in Figure 5. During

the sampling process, the pH value of each sample was measured immediately on-site to avoid errors. The measurement was repeated three times, and the average value was taken as the final result. To preserve the surface water samples for laboratory testing, protective agents were added to the samples.
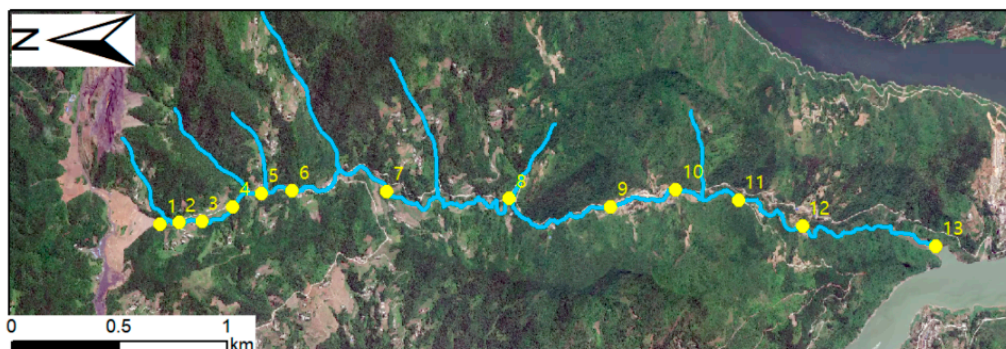
Figure 3. Distribution map of sampling points.

(**a**)   (**b**)

Figure 4. Current status of mining operations and surface water pollution in the study area: (**a**) collect water samples; and (**b**) measure the pH of the water samples.

(**a**)   (**b**)

Figure 5. Photos of the collected sediments: (**a**) upstream sediment samples; and (**b**) downstream sediment samples.

2.2.1. Testing of Surface Water Samples

In this study, the DGB-480 Multi-Parameter Water Quality Analyzer (produced by INESA (Group) Co., Ltd., Shanghai, China) was used to measure the content of Fe, Al, Mn, Zn, Ni, Pb, Cl^- and SO_4^{2-} elements in the water. This product employs an 8-wavelength optical measurement system and a 90-degree light-scattering turbidity detection optical path, with over 40 built-in detection items and methods that can be directly accessed for fast and convenient measurements. The instrument comes with a complementary Leici special reagent kit for flexible use. The testing of the water samples was completed in the university laboratory, which is equipped with the DGB-480 Multi-Parameter Water Quality Analyzer and its accompanying digester, capable of detecting the concentrations in water. The testing methods are listed in Table 1. To measure the redox potential (Eh) of the water quality using an ORP meter, the instrument has a measurement range of ± 1100 mV, a resolution of 1 mV, and an accuracy of ± 15 mV.

Table 1. Water quality testing methods.

Serial Number	Detection Instrument	Method	Measurement Range (mg/L)	Detection Reagent
Fe	DGB-480 multi-parameter water quality analyzer, digestion apparatus	Phenanthroline method	0.025–5.00	Iron color reagent, iron reagent A, iron reducing agent powder, ferrous ion standard solution
Al	DGB-480 multi-parameter water quality analyzer	Chrome azurol S spectrophotometric method	0.005–0.300	Aluminum buffer solvent, aluminum buffer powder, aluminum color reagent, aluminum standard solution
Cl^-	DGB-480 multi-parameter water quality analyzer	Mercury thiocyanate method	1.000–100.0	Chloride reagent A, chloride reagent B, chloride standard solution
SO_4^{2-}	DGB-480 multi-parameter water quality analyzer	Barium sulfate turbidimetry	0.5–100	Stabilizer solution, barium chloride powder, sulfate calibration solution
Mn	DGB-480 multi-parameter water quality analyzer	High iodic acid oxidation method	0.1–20.0	Manganese determination reagent, manganese color reagent, manganese standard solution
Zn	DGB-480 multi-parameter water quality analyzer	Zinc reagent method	0.05–5.00	Zinc reagent, zinc standard solution
Ni	DGB-480 multi-parameter water quality analyzer	Dimethylglyoxime method	0.05–10.00	Nickel reagent, nickel standard solution
Pb	DGB-480 multi-parameter water quality analyzer	TPPS method	0.025–1.000	Lead alkaline solution, lead color reagent, lead calibration liquid

To ensure the accuracy and reliability of the test results, parallel samples need to be set up for measurement, and the relative deviation of the measurements should not exceed 20%. During the experiment, if the measured value of a sample exceeds the measurement range, indicating an inaccurate result, the sample must be diluted proportionally until an accurate measurement is obtained.

2.2.2. Testing of River Sediments

This experiment was conducted by the Experimental Testing Laboratory of Xi'an Geological Survey Center, China Geological Survey, using a field emission scanning electron

microscope with the model number JEOL JSM-7500F (produced by JEOL Co., Ltd., Tokyo, Japan). This equipment primarily utilizes secondary electron signal imaging to observe the surface morphology of samples. It features an acceleration voltage ranging from 0.1 kV to 30 kV, a resolution of 1.0 nm (at 15 kV)/1.4 nm (at 1 kV), and a magnification factor of $25\times$ to 1 million times. Equipped with an X-ray energy dispersive spectrometer (EDS), it enables simultaneous observation of microstructures and analysis of micro-area compositions. The testing capabilities include optical section scanning, 3D image processing, time-series scanning imaging, wavelength-series scanning imaging; observation and analysis of cells, green fluorescent proteins, and biological fluorescent samples; as well as fluorescence in situ hybridization analysis. Its primary applications encompass microscopic morphological observation and fracture morphology analysis of materials such as metals, non-metals, semiconductors, minerals, metallurgy, and archaeological artifacts. Additionally, it provides high-resolution imaging of samples and micro-area composition analysis in conjunction with EDS.

The experiment utilized the Oxford X-Max50 energy dispersive spectrometer (EDS) and JFC-1600 Ion Sputter, both manufactured by Oxford Instruments Co., Ltd., London, UK. The Oxford X-MaxN50, an electrically cooled EDS from Oxford Instruments, was integrated with the field emission scanning electron microscope for the analysis of elemental species and their concentrations in the micro-regions of materials. This combination supports the use of both scanning electron microscopy (SEM) and transmission electron microscopy (TEM). The large-area silicon drift detector (SDD) EDS technology offers superior analytical performance, featuring enhanced resolution capabilities where even an 80 mm^2 detector can achieve 123 eV (MnKa) resolution. It boasts high-speed capabilities with a sensitivity equivalent to 15 times that of a traditional 10 mm^2 electrically cooled detector.

The portable ground spectroradiometer (FieldSpec 4 Hi-Res, Analytica Spectra Devices, Inc., Boulder, CO, USA) was utilized to measure the visible to near-infrared spectral range (350–2500 nm) of river sediments. It employs a 512-element array, a PDA detector, and two independent InGaAs detectors, enabling rapid and non-destructive acquisition of spectra across the wavelength range of 350 to 2500 nm. The FieldSpec 4 Hi-Res primarily consists of a laptop computer, the main observation unit, a pistol-grip handle, a fiber-optic probe, connecting cables, and a calibration white panel. Before taking measurements, power on the spectroradiometer and the laptop computer, and launch the RS3 software (version 1.1). After loading the instrument's startup system, it is necessary to calibrate the instrument using the white panel before each spectral acquisition, with the instrument probe oriented vertically downwards. Prior to taking measurements, the spectroradiometer requires a warm-up period of 15 min [31].

The handheld X-ray fluorescence (XRF) analyzer was used to measure the elements on the surface of sediments. By acquiring spectral data within the wavelength range of 350 to 2500 nm, the analyzer provides information about the elemental composition.

The crystal phase composition of the white precipitate sample was analyzed by XRD (D2 PHASER, Bruker, Billerica, MA, USA). The instrument was operated at 37.5 kV and 20 mA with Cu-Kα1 radiation (k = 0.154 nm). XRD data were collected in the scanning range of $2\theta = 5$–$70°$, and the spectra were scanned at a speed of $4° \, min^{-1}$ (2θ) with a step of $0.02°$. During the experimental process, the samples were thoroughly ground into fine powders to ensure that X-rays could uniformly irradiate every part of the samples, thus obtaining representative data. The diffraction patterns obtained during the measurement were converted into intensity-2θ curves. Based on the displacement and intensity of these diffraction peaks, the crystalline phases in the samples could be identified, and qualitative analysis was conducted by comparison with standard databases.

To further verify the chemical compositions of the yellow and white precipitates, we utilized the PHREEQC geochemical software (version 1.1) to develop a detailed geochemical model. This model enabled us to more accurately simulate the conditions under which the precipitates formed and conduct in-depth analysis of their mineral compositions. The specific steps are outlined below. Firstly, we utilized chemical data from sediment samples and water samples. These data included the ion concentrations in the water and the major elements and chemical components in the sediments. These data served as the necessary input for establishing the model. Next, using the geochemical simulation capabilities of the PHREEQC software, we calculated the saturation indices (SIs) of different minerals. The saturation index refers to the ratio of the solubility of a mineral under specific water chemical conditions to the concentration of the mineral solute in the water. If the saturation index is greater than 0, it indicates that the water is supersaturated and the mineral may precipitate out; if the saturation index is less than 0, it suggests that the water is undersaturated and the mineral is unlikely to precipitate.

2.2.3. Evaluation Methods for Surface Water

Calculating the individual pollution over-limit multiples of water quality can reveal the over-limit conditions of Fe and Al [32]. The formula for calculating the individual pollution over-limit multiple (Pi) is:

$$P_{Ci} = \frac{C_i}{S_i},\tag{1}$$

In the formula, C_i represents the measured concentration (mg/L) of the ith water quality indicator; and S_i represents the evaluation standard (mg/L) for the ith water quality indicator. The study area belongs to the Han River water system, and the surface water functional zoning is classified as Class II water. Therefore, the evaluation was conducted according to the pollutant limits for Class II water specified in the "Environmental Quality Standards for Surface Water (GB3838-2002)". The standard limit for Category II water for Fe is 0.2, the standard limit for Category II water for Al is 0.05, the standard limit for Category II water for Mn is 0.1, the standard limit for Category II water for Zn is 1.0, the standard limit for Category II water for Ni is 0.02, and the standard limit for Category II water for Pb is 0.01. The normal range of pH values for surface water is between 6 and 9. The pollution levels of Fe and Al in river water are classified into the following four grades (Table 2).

Table 2. Classification of water quality based on individual pollution over-limit multiples.

Evaluation Criteria	Level of Pollution
$PCi \leq 0$	Unpolluted
$0 < PCi \leq 1$	Slightly Polluted
$1 < PCi \leq 4$	Moderately Polluted
$4 < PCi \leq 10$	Heavily Polluted
$10 < PCi$	Extremely Polluted

3. Results

3.1. Experimental Results of Surface Water Samples

Spectrophotometry was used to measure the content of Fe, Al, Cl^-, SO_4^{2-}, Mn, Zn, Ni and Pb ions in the water. During the testing process, each sample was measured three times repeatedly, and the average value was taken as the final measurement result. As can be seen from the test results (Table 3), the pH value range is between 3.16 and 4.47, indicating an overall acidic condition. The pH value of the water samples gradually increases from upstream to downstream. Both the Fe and Al ion content in the water samples shows

an overall decreasing trend from upstream to downstream. It is initially determined that the decreasing content of Fe and Al ions in the water is due to their conversion into iron and aluminum deposits. The concentration of Cl^- does not exhibit any obvious pattern and remains unreacted in acidic water. The content of SO_4^{2-} shows an overall decreasing trend from upstream to downstream. The overall trend for the concentrations of Mn, Zn, Ni, and Pb heavy metal ions is also higher at upstream locations and lower at downstream locations. The Eh values decrease sequentially from upstream to downstream.

Table 3. The test results of the surface water samples.

Sample	pH	Eh (mV)	Fe (mg/L)	Al (mg/L)	Cl^- (mg/L)	SO_4^{2-} (mg/L)	Mn (mg/L)	Pb (mg/L)	Ni (mg/L)	Zn (mg/L)
1	3.22	261	4.66	0.280	11.0	29.9	36.5	1.22	5.86	0.401
2	3.16	268	3.74	0.142	3.39	25.6	32.3	1.30	0.666	1.05
3	3.40	254	2.70	0.262	39.9	21.1	29.4	1.12	1.54	1.46
4	3.46	233	2.07	0.176	3.39	16.9	22.3	0.954	1.69	1.26
5	3.45	241	2.41	0.192	2.11	19.6	22.5	1.09	1.16	2.04
6	3.84	230	0.560	0.135	3.64	13.5	15.1	0.84	0.310	1.62
7	4.06	224	0.781	0.116	11.8	12.0	15.7	0.883	0.636	3.10
8	4.16	201	0.574	0.140	3.36	10.5	14.1	0.800	0.548	1.44
9	4.19	198	0.429	0.0990	3.29	10.2	14.3	0.826	0.745	0.960
10	4.21	194	0.477	0.103	1.68	9.57	13.1	0.763	0.690	1.02
11	4.37	187	0.392	0.0900	3.98	8.74	13.6	0.933	0.691	1.41
12	4.26	189	0.292	0.0910	4.03	8.13	13.5	0.775	0.588	1.46
13	4.47	142	0.206	0.0870	1.89	7.46	10.4	0.907	0.604	0.737

At the same time, parallel samples of the primary research subjects, Fe and Al, were also measured, two parallel samples were selected for each sample index for detection, and the relative deviation was within the allowable range (Tables 4 and 5).

Table 4. Measurement of iron parallel samples.

Sample	Fe (mg/L)	Relative Deviation
3	2.81	0.020
10	0.451	0.0280

Table 5. Measurement of aluminum parallel samples.

Sample	Al (mg/L)	Relative Deviation
2	0.153	0.0370
7	0.122	0.0250

3.2. Sediment Test Results

Under the scanning electron microscope, different minerals exhibit distinct morphologies. The microscopic morphology diagrams of the target minerals observed under the electron microscope are shown in Figure 6. Figure 6a represents Sample No. 1 from upstream, and Figure 6b represents Sample No. 9 from downstream. It can be seen that the morphology of Sample No. 1 consists of numerous short needle-like structures piled together, as shown in Figure 6a, while the morphology of Sample No. 9 comprises a stack of flaky structures, as depicted in Figure 6b. Based on the morphology, it is inferred that the upstream samples are iron-bearing deposits, and the downstream samples are aluminum-bearing deposits [33]. In other words, among the 13 samples, Samples No. 1–8 are iron-bearing deposits, and Samples No. 9–13 are aluminum-bearing deposits.

The secondary electron spectra of the target minerals are shown in Figure 7. Figure 7a presents the secondary electron spectrum of the upstream samples, where the peak intensity of Fe ions is significantly higher than that of Al ions. Figure 7b displays the secondary electron spectrum of the downstream mineral samples, where the peak intensity of Al ions is notably higher than that of Fe ions. The results of the mass percentage (wt%) of the elemental composition of the samples are shown in Table 6. It can be observed that the relative content of Fe ions in the sediments generally decreases from upstream to downstream, with Sample No. 1 having the highest relative content of Fe ions and Sample No 11 having the lowest. Conversely, the relative content of Al ions increases overall, with Sample No. 2 having the lowest relative content of Al ions and Sample No. 10 having the highest. Samples No. 1–8 contain more Fe ions than Al ions, while Samples No. 9–13 contain more Al ions than Fe ions. This also confirms that the upstream sediments are primarily iron-bearing deposits, while the downstream sediments are primarily aluminum-bearing deposits.
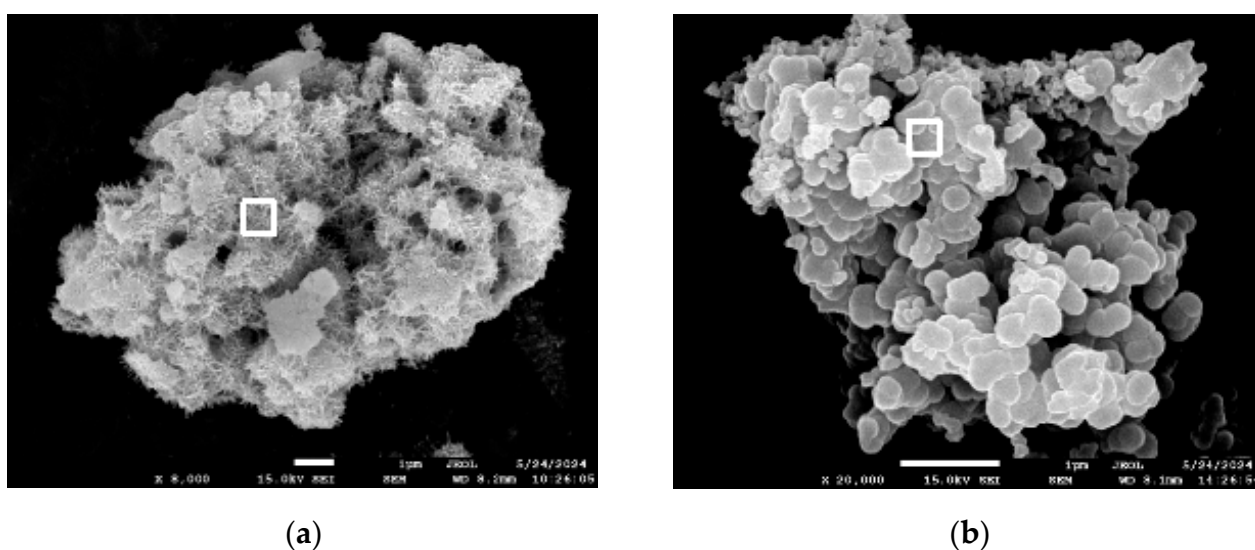

(**a**)　　　　　　　　　　　　　　　　　　　　　　　　　　(**b**)

Figure 6. Microscopic morphology of target minerals in the sample: (**a**) microscopic morphology diagram of upstream samples; and (**b**) microscopic morphology diagram of downstream samples.

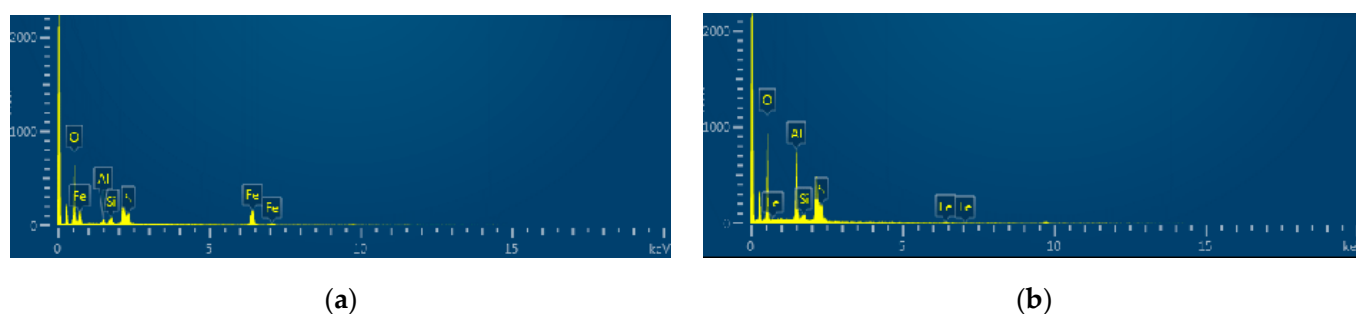
(**a**)　　　　　　　　　　　　　　　　　　　　　　　　　　(**b**)

Figure 7. Secondary electron spectroscopy image of target minerals in the sample: (**a**) secondary electron spectrogram of upstream sample minerals; and (**b**) secondary electron spectroscopy image of downstream sample minerals.

The significant variations in the mass percentage (wt%) of Fe and Al ions in the river sediments across different map locations are illustrated in Figures 8 and 9. The color gradient from dark to light in the maps reflects the decrease in ion mass from high to low. Figure 8 shows a gradual lightening of the point colors from upstream to downstream, indicating a sequential decrease in the mass of Fe ions. Conversely, Figure 9 depicts a grad-

ual darkening of the point colors from upstream to downstream, indicating a sequential increase in the mass of Al ions.

The spectral data obtained from the sediment samples are presented in Figure 10. These data were compared with the visible and near-infrared spectral data of goethite and alunite downloaded from the USGS database. The dashed lines in the figure indicate where the sample spectral curves exhibit identical absorption characteristics to the reference spectral curves. The results show that the spectral curves of the samples numbered 1 to 8 were consistent with those of goethite, while the spectral curves of the samples numbered 9 to 13 matched those of alunite.

Table 6. Mass percentage of elements in the minerals.

Sample	Fe (wt%)	Al (wt%)	O (wt%)	Si (wt%)	S (wt%)
1	50.7	2.26	42.5	2.08	0
2	48.2	1.01	47.5	0	3.27
3	50.9	1.05	43.4	1.23	3.38
4	53.7	2.19	37.9	1.98	4.14
5	51.2	2.93	33.4	4.68	6.98
6	44.7	6.28	42.7	1.63	4.75
7	47.9	4.82	13.2	0	6.48
8	39.3	14.2	35.1	6.65	4.70
9	2.45	28.5	63.9	1.83	3.24
10	4.76	28.7	63.5	3.07	0
11	0	32.6	60.9	0	2.74
12	1.67	27.9	61.6	2.84	6.01
13	2.22	27.0	61.7	5.36	0

Figure 8. Variation map of the Fe mass percentage (wt%) in river sediments.
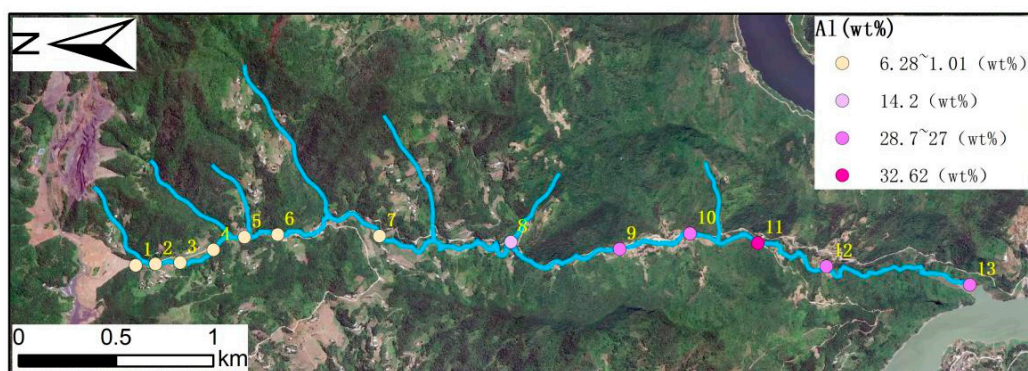

Figure 9. Variation map of the Al mass percentage (wt%) in river sediments.

The measurement results obtained using the handheld X-ray XRF analyzer are shown in Table 7. The Pb content ranges from 13.6 mg/kg to 41.2 mg/kg, the Mn content ranges from 1526 mg/kg to 45.7 mg/kg, the Ni content ranges from 1479.8 mg/kg to 20.4 mg/kg, and the Zn content ranges from 199.4 mg/kg to 38.7 mg/kg.
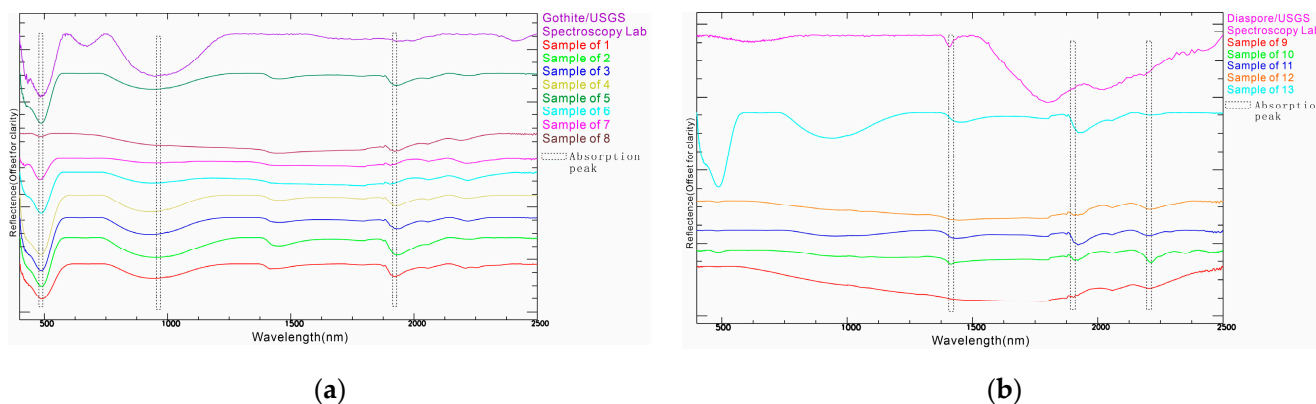
(**a**)

(**b**)

Figure 10. The spectral curves of the samples: (**a**) the spectral curves of the samples numbered 1 to 8; and (**b**) the spectral curves of the samples numbered 9 to 13.

Table 7. Measurement results obtained from the X-ray fluorescence (XRF) analyzer.

Sample	Mn (mg/kg)	Ni (mg/kg)	Zn (mg/kg)	Pb (mg/kg)
1	1562	1479.8	50.7	41.2
2	1149.3	1101.2	94.7	15.8
3	1711.6	2274.6	70.9	15.6
4	1090.3	965.1	64.5	15.1
5	1229.6	615.5	63.5	14.9
6	662.9	385.3	78.7	14.6
7	942.1	1070.3	64.1	14.2
8	670.6	312.2	62	16.0
9	45.7	268.9	61.7	15.7
10	621.2	127.4	38.7	14.0
11	965.9	794.3	199.4	13.6
12	791.6	1432.3	128.9	15.5
13	416.9	20.4	127.7	13.6

Samples from both the upstream and downstream locations were selected for XRD analysis, specifically Sediment Sample No. 1 from the upstream and Sediment Sample No. 10 from the downstream. The spectra are shown in Figure 11. A comparison with the POWDER X-RAY DIFFRACTION database on the RRUFF project website (https://rruff.info/, accessed on 8 January 2024) revealed that the spectrum of the upstream sediment is most similar to goethite, while the spectrum of the downstream sediment is most similar to diaspore. These results are consistent with the spectral analysis results obtained by ESM.

The results of the geochemical model established using PHREEQC software are presented in Table 8. From the table, it can be observed that from upstream to downstream at points 1–13, the Fe and Al in the solution gradually reach saturation, leading to the formation of yellow and white precipitates. Among these precipitates, the primary mineral phase of the yellow precipitate is hematite, while the main mineral phase of the white precipitate is boehmite.
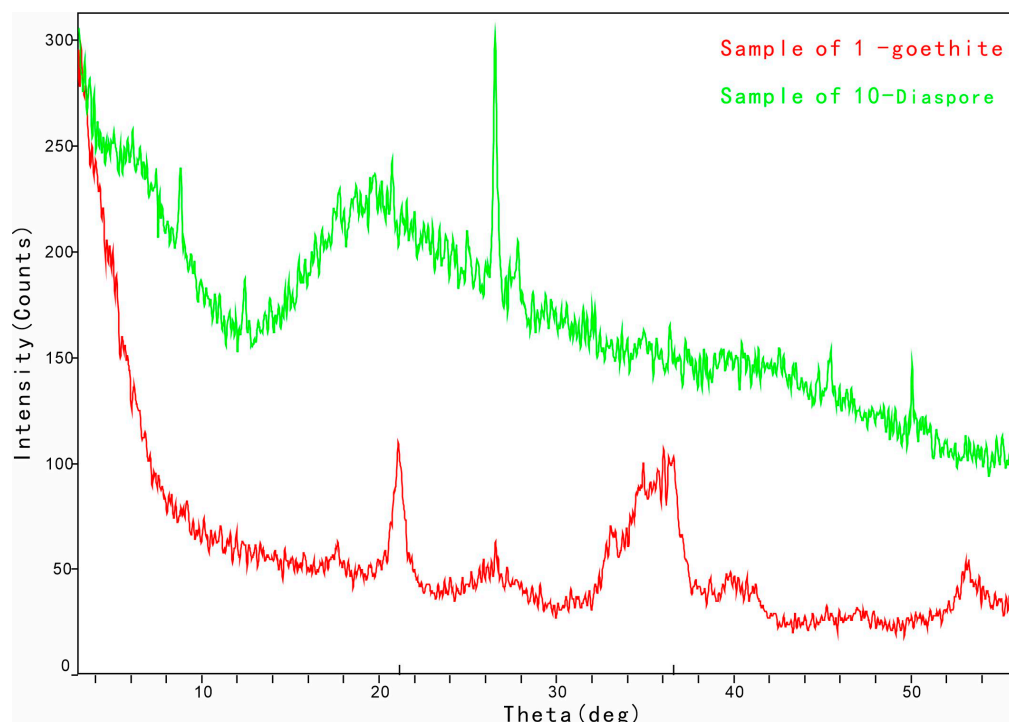
Figure 11. XRD spectra of Fe and Al in sediment samples.

Table 8. The results of the mineral phase simulation using PHREEQC software.

Chemical Formula	Phase	Sample												
		1	2	3	4	5	6	7	8	9	10	11	12	13
Fe_2O_3	Hematite	−2.48	−2.48	−1.86	−1.69	−1.62	−0.523	1.07	1.42	1.35	1.57	2.36	1.44	2.41
AlOOH	Diaspore	−2.28	−2.28	−1.73	−1.68	−1.69	−0.636	−0.0574	0.331	0.269	0.350	0.740	0.446	1.01
FeOOH	Goethite	−2.25	−2.25	−1.94	−1.86	−1.83	−1.27	−0.475	−0.301	−0.336	−0.227	0.166	−0.290	0.194
Al(OH)3	Gibbsite	−3.53	−3.53	−2.98	−2.93	−2.94	−1.88	−1.31	−0.922	−0.984	−0.903	−0.513	−0.807	0.241
$Fe(OH)_{2.7}Cl_{0.3}$	$Fe(OH)_{2.7}Cl_{0.3}$	−2.41	−2.41	−1.99	−2.24	−2.27	−1.76	−0.877	−0.895	−0.943	−0.927	−0.469	−0.891	0.567
AlOOH	Boehmite	−3.94	−3.94	−3.39	−3.34	−3.35	−2.29	−1.72	−1.33	−1.39	−1.31	−0.922	−0.216	0.650

3.3. Evaluation Results of Surface Water

The individual pollution exceedance multiples of the heavy metals in the water, as measured according to the formula, are shown in Table 9.

As can be seen from the above table, the calculated results of the individual pollution exceedance multiples of Fe and Al are both greater than 0, indicating that varying degrees of pollution exist at all 13 sampling points. For Fe ions, sampling points 5, 12, and 13 are mildly polluted; sampling points 7, 8, 9, 10, and 11 are moderately polluted; sampling point 4 is severely polluted; and sampling points 1, 2, 3, and 6 are extremely polluted. For Al ions, sampling points 5, 10, 12, and 13 are mildly polluted; sampling points 2, 4, 6, 7, 8, 9, and 11 are moderately polluted; and sampling points 1 and 3 are severely polluted. The calculation results for the individual pollution exceedance multiples of Mn, Pb, and Ni are all greater than 10, indicating that the pollution levels of these three heavy metals are extremely severe. In contrast, the pollution level of Zn is relatively low, with sites 1, 9, and 13 being unpolluted, sites 5 and 7 experiencing moderate pollution, and all the other sites suffering from mild pollution. The overall water quality in the study area is acidic, with a pH range of 3.16 to 4.47. The normal range of the pH for surface water is between 6 and 9. Therefore, the overall pH values in the study area exceed the standard, confirming that the problem of acidic water in the study area is severe.

Table 9. Exceedance of heavy metal ions in water quality.

Sample	Exceedance Multiples of Fe	Exceedance Multiples of Al	Exceedance Multiples of Mn	Exceedance Multiples of Pb	Exceedance Multiples of Ni	Exceedance Multiples of Zn
1	22.3	4.60	729	121	2929	−0.600
2	17.7	1.84	645	129	332	0.0400
3	12.5	4.24	587	111	769	0.460
4	9.33	2.52	445	94.4	847	0.260
5	11.1	2.84	449	109	579	1.04
6	1.80	1.70	301	83.0	154	0.620
7	2.91	1.32	313	87.3	317	2.10
8	1.87	1.80	281	79.0	273	0.440
9	1.15	0.980	284	81.6	372	−0.0400
10	1.39	1.06	261	75.3	344	0.0200
11	0.960	0.800	272	92.3	345	0.410
12	0.460	0.820	268	76.5	293	0.460
13	0.030	0.470	206	89.7	301	−0.260

4. Discussion

It is found that the sulfur–iron mining areas in Baihe County, Lueyang County, Xixiang County, Zhenba County, and other places in the Qinba Mountains, molybdenum mining areas in Luonan County, gold mining areas in Hanyin County, and Haopinghe stone coal mining areas all have significant "yellow precipitate" pollution in rivers caused by iron and manganese pollution [34]. In the study of acidic water in pyrite belts in Iberia, the research area also showed the phenomenon of "yellow precipitate" pollution [35]. Some white precipitates can be seen in some creeks in the molybdenum mining area of Jinduicheng, Shaanxi Province [36]. Similar white precipitates were also found in the acid mine drainage in the Paradise Mine in the United States and the Dabaoshan polymetallic mining area in Guangdong Province [37]. However, the evolution from upstream acidic "yellow precipitate" to downstream acidic "white precipitate" was only found in the Xiaomixi Stream basin, so it has research significance.

4.1. Distribution of Fe and Al Ions in Surface Water

By evaluating the current status and extent of the water pollution within the study area, it has been determined that the pollution exceeds the Class II standards of the "Groundwater Quality Standards" (GB/T14848-17), posing a significant risk of surface water pollution. Apart from the risks posed to human health, this pollution also seriously threatens the water quality and safety of the Han River. Studies have found that due to the interaction between acidic water and carbonate rocks, the pH and alkalinity gradually increase with the increase in the flow path distance, while the concentrations of SO_4^{2-}, Fe^{2+}, and Al^{3+} decrease due to the deposition of secondary carbonate rocks [38].

This study employed spectrophotometry to systematically quantify the concentrations of Al, Cl^-, SO_4^{2-}, Mn, Zn, Ni and Pb ions in surface water, revealing significant patterns in the variations of these key water quality indicators along the river's hydrological pathway. The experimental results indicate that, from upstream to downstream of the river, the pH value of the river exhibits an increasing trend, while the concentrations of Fe, Al, and SO_4^{2-} ions show a consistent decreasing trend. As illustrated in Figure 12, as the pH increases, the concentrations of Fe, Al, and SO_4^{2-} ions in the water decrease [39]. The Eh values decrease sequentially from upstream to downstream. The pH value is an important factor influencing the Eh. Generally speaking, the higher the pH value, the lower the Eh; conversely, the lower the pH value, the higher the Eh [40]. Concurrently, we observed the spatial evolution of the river from "yellow precipitate" to "white precipitate", discovering that iron precipitates significantly before aluminum. Preliminary speculation suggests that the reduction in SO_4^{2-} may be due to the interaction with carbonate rocks ($CaCO_3$, $CaMg(CO_3)_2$), leading to the precipitation and subsequent depletion of the SO_4^{2-} concentration as a result of the deposition of secondary minerals. Alternatively, it may

be diluted during the flow of the river [41]. This discovery provides important clues for understanding the migration and transformation processes of metal ions in river systems.
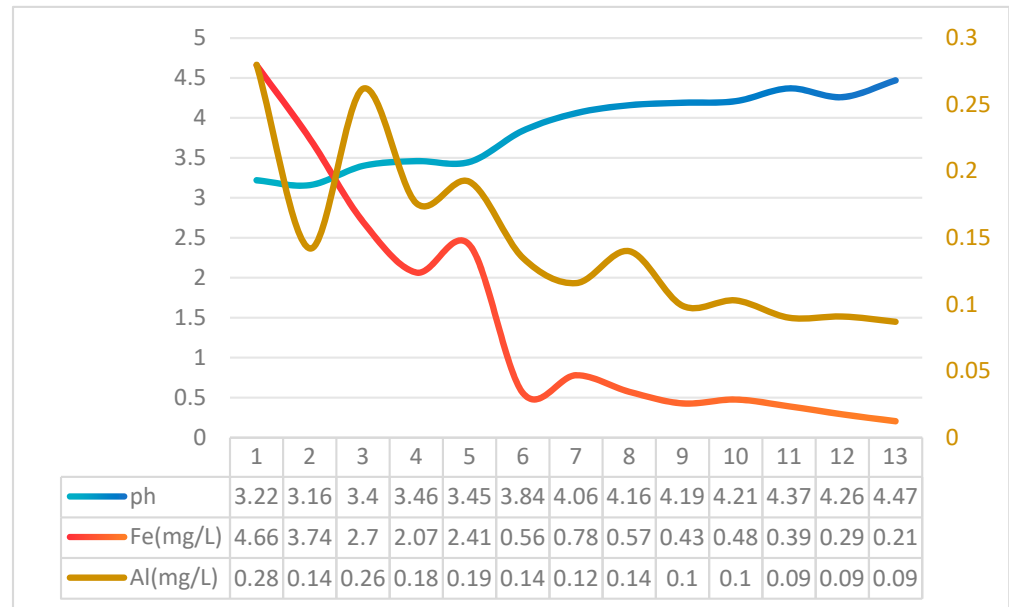

	1	2	3	4	5	6	7	8	9	10	11	12	13
ph	3.22	3.16	3.4	3.46	3.45	3.84	4.06	4.16	4.19	4.21	4.37	4.26	4.47
Fe(mg/L)	4.66	3.74	2.7	2.07	2.41	0.56	0.78	0.57	0.43	0.48	0.39	0.29	0.21
Al(mg/L)	0.28	0.14	0.26	0.18	0.19	0.14	0.12	0.14	0.1	0.1	0.09	0.09	0.09

Figure 12. Results of the Fe and Al ion content in the surface water experiments.

Furthermore, by calculating the individual pollution exceedance multiples of heavy metal ions in the water, we conducted an in-depth assessment of the current status and extent of water pollution within the study area. The results indicate that the concentrations of heavy metal ions in the study area generally exceed the established water quality standards, revealing varying degrees of pollution. Specifically, the upstream areas of the rivers have been particularly severely affected by pollution, with concentrations reaching levels of extreme and heavy pollution; however, as the water flows downstream, the degree of pollution gradually diminishes. Given that the sampling starting point is located near an abandoned coal mine, the pyrite- and aluminum-bearing minerals in the mining waste residue come into contact with oxygen and water, leading to severe upstream pollution. These findings not only emphasize the importance of controlling pollution sources in the upstream of the river but also provide a scientific basis for formulating effective water environmental protection strategies and implementing targeted remediation measures [42,43].

4.2. Migration of Fe and Al Ions in Sediment

During the formation and evolution of AMD, Fe and Al ions undergo a series of reactions, resulting in the production and precipitation of some relatively insoluble secondary minerals, such as hydroxysulfates and hydroxides [44]. The geochemical behavior of Fe and Al mainly controls the mobility of metals through adsorption and coprecipitation in the acidic sulphate water [45].

The above findings indicate that iron precipitates significantly before aluminum in the river. The morphology and composition characteristics of the sediment samples were analyzed through SEM-EDS, revealing the laws of metal ion migration and transformation processes in the river system. The SEM-EDS analysis results show that the main components of the sediment samples are O, Al, Fe, S, and Si (Figure 7). In Sample 1, the mass percentage of the metal ions shows Fe > Al, while in Sample 9, the mass percentage is Al > Fe (Figure 7b). According to the statistics, the changes in the mass percentages of Fe and Al in the sediments of the 13 samples are shown in Figure 13. Combining the differences in the mineral micro-morphology diagrams (Figure 6), it can also be concluded that the

upstream yellowish–brown sediments are iron-bearing sediments (Figure 6a), while the downstream white sediments are aluminum-bearing sediments (Figure 6b) [46]. When the pH is less than 4.16, Samples 1–8 are mainly iron-bearing sediments, and when the pH is greater than 4.16, Samples 9–13 are mainly aluminum-bearing sediments in the river. Therefore, the surface water in the study area spatially exhibits an evolution process from acidic "yellow precipitate" to acidic "white precipitate" [34]. The test results from the ASD spectral scanner, when compared with the visible and near-infrared spectral data of goethite and alunite, also confirm that the samples numbered 1 to 8 are iron-bearing sediments, and the samples numbered 9 to 13 are aluminum-bearing sediments. This is consistent with the analysis results obtained from SEM-EDS. The above conclusions were also confirmed through XRD testing, with the upstream being iron-bearing sediments and the downstream mainly aluminum-bearing sediments.

	1	2	3	4	5	6	7	8	9	10	11	12	13
Fe (wt%)	50.76	48.22	50.92	53.72	51.17	44.69	47.87	39.31	2.45	4.76	0	1.67	2.22
Al (wt%)	2.26	1.01	1.05	2.19	2.93	6.28	4.82	14.2	28.54	28.7	32.62	27.92	27
ph	3.22	3.16	3.4	3.46	3.45	3.84	4.06	4.16	4.19	4.21	4.37	4.26	4.47
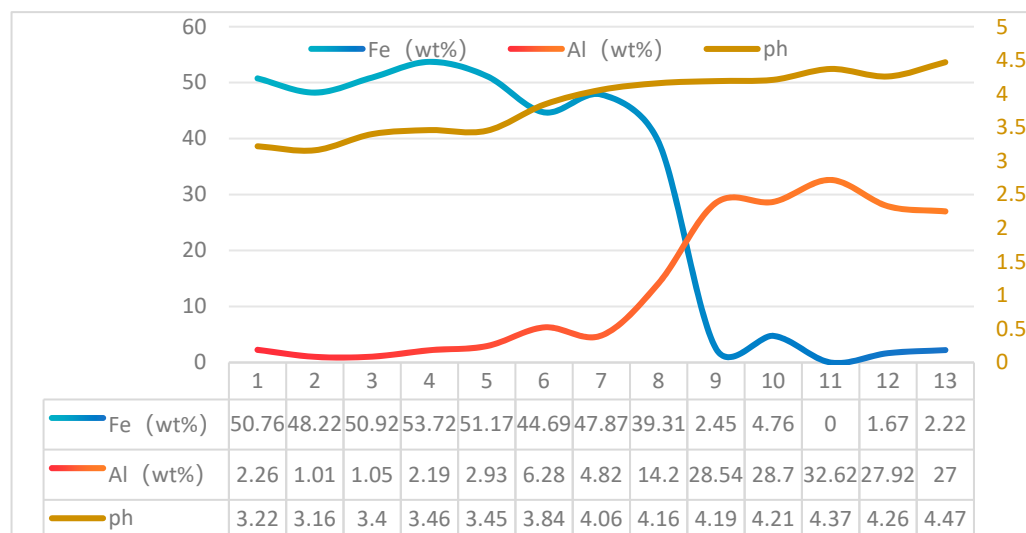
Figure 13. Mass percentage of Fe and Al ions in the river sediments.

This experimental result also provides a basis for the surface water test results, as the transformation of Fe and Al ions into iron-bearing sediments and aluminum-bearing sediments during the downstream progression of the river leads to a decreasing trend in the concentrations of Fe and Al ions in the surface water from upstream to downstream.

Based on Table 6, it can be observed that there are no ions in the sediments (such as Ca^+ and Mg^{2+}) capable of reacting with SO_4^{2-} to form precipitates. Therefore, it can be determined that the decrease in the SO_4^{2-} concentration from upstream to downstream in the river is due to dilution in the water. To verify this phenomenon, the Fe and Al concentrations and pH values in the tributaries flowing into the Xiaomi Stream were examined. The distribution of sampling points for the tributaries is shown in the Figure 14. The Fe and Al content and pH values of each tributary are shown in Table 10. The results show that the concentrations of Fe and Al in the tributaries were significantly lower than those in the main stream, and the pH values of the water were within the normal range, indicating that the water quality of the tributaries was much better than that of the main stream. Consequently, the inflow of tributaries leads to the dilution of SO_4^{2-} ions in the water, resulting in a gradual decrease in their concentration.
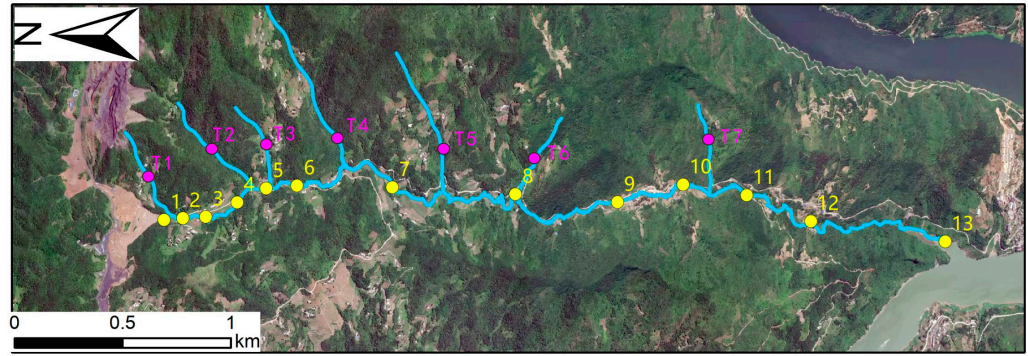
Figure 14. Illustration of the sampling points for the tributaries.

Table 10. The Fe and Al content, as well as the pH value, of the tributaries.

Sample	pH	Fe (mg/L)	Al (mg/L)
T1	6.28	0.254	0.0880
T2	6.15	0.170	0.0730
T3	6.63	0.164	0.0720
T4	7.57	0.244	0.00700
T5	8.05	0.140	0.0680
T6	7.44	0.250	0.0180
T7	6.31	0.106	0.0650

4.3. The Migration and Transformation Mechanism of Fe and Al Ions in Acidic Water

The behavior of iron and aluminum in acid mine drainage (AMD) has been thoroughly studied during the last three decades [47] and the minerals controlling their solubility have been identified and investigated in detail [48]. Thus, ferric iron is known to be mostly dissolved under very acidic conditions (pH < 2), and above this pH, Fe is usually hydrolyzed and precipitated as different ochreous minerals. Aluminum is generally conservative below pH 4.5–5.0 and tends to precipitate in the form of several hydroxysulfates when the pH is higher than that [49]. Such Fe(III) and Al speciation has important implications for the geochemical evolution of AMD.

The experimental results show that the migration and transformation process of metal ions is closely related to the pH value of the river. The river is generally acidic, with a pH range of 3.16 to 4.47, increasing gradually from upstream to downstream. The pH value of the river increases from 3 to 4 at point 8, and it is precisely at this location that the main component in the sediment changes from Fe to Al. In other words, when the pH is less than 4.16, the river is dominated by iron-bearing sediments, and when the pH is greater than 4.16, the river is dominated by aluminum-bearing sediments.

The generation of acidic water in mines is the result of the exposure and rapid oxidation of sulfide minerals associated with abandoned coal and metal mines [50]. Combined with the EDS results, it can be seen that in addition to the main components of Fe and Al, the sediment composition also contains S, which also indicates that the main mineral causing acidic water pollution in the study area is pyrite [51]. Under normal circumstances, pyrite will undergo the following reaction to generate iron hydroxide precipitate, which appears yellowish–brown. Pyrite is oxidized by the action of oxygen and water:

$$FeS_2 + 7/2O_2 + H_2O = Fe^{2+} + 2SO_4^{2-} + 2H^+ \tag{2}$$

Under sufficient oxygen conditions, ferrous sulfate will be converted into ferric sulfate:

$$Fe^{2+} + 1/4O_2 + H^+ = Fe^{3+} + 1/2H_2O \tag{3}$$
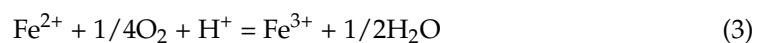
In an acidic environment, ferric sulfate undergoes the following further reaction:

$$Fe^{3+} + 3H_2O = Fe(OH)_3 + 3H^+ \qquad (4)$$
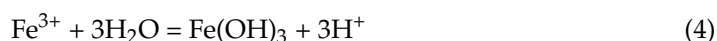
The aluminum in mine acidic water comes from the oxidation of aluminum secondary minerals in the symbiotic or associated environment. The most common aluminum secondary mineral is alunite ($KAl_3(SO_4)_2(OH)_6$) [52], which undergoes the following reaction in water to form aluminum hydroxide precipitate, appearing milky white.

$$KAl_3(SO_4)_2(OH)_6 = k^+ + 3Al^{3+} + 2SO_4^{2-} + 6OH^- \qquad (5)$$

$$Al^{3+} + 3H_2O = Al(OH)_3 + 3H^+ \qquad (6)$$
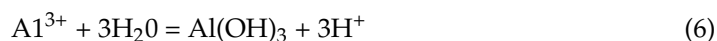
This study found that the content of Al in acidic mine water is relatively high when the pH is less than 4.16, while when the pH is greater than 4.16, Al is mainly distributed on the surface of minerals, forming aluminum hydroxide precipitate [19].

To further verify the chemical compositions of the yellow and white precipitates, a geochemical model was established using PHREEQC software. Based on the chemical data of the water samples and sediments, the saturation indices of the minerals were calculated to analyze the possible mineral compositions [36]. During the simulation, it was found that both Fe and Al reached saturation states in the solution, indicating the formation of precipitates. In contrast, Mn, Pb, Ni, and Zn did not reach saturation in the simulation, remaining in solution. According to the abundance of chemical elements in the Earth's crust, the contents of Mn, Pb, Ni, and Zn detected by X-ray fluorescence (XRF) were trace amounts. Therefore, these elements did not reach saturation in the calculation results and did not form precipitates, instead adsorbing onto the surfaces of other minerals. Ultimately, based on the results of our model, we conclude that from upstream to downstream at points 1–13, the Fe and Al in solution gradually reach saturation, leading to the formation of yellow and white precipitates. Among these, the primary mineral phase of the yellow precipitate is hematite, while the main mineral phase of the white precipitate is boehmite. Through these analyses, we have not only verified the mineral composition of the precipitates but also further elucidated the influence of geochemical conditions on mineral precipitation. This provides an important basis for subsequent mineralogical studies and water quality improvement.

The above experimental results demonstrate that the migration and transformation processes of Fe and Al ions in acidic water are closely related to the pH value of the river, and the pH conditions for the presence of iron and aluminum precipitates are different [19], with their compositions being unstable. This study found that when the pH is less than 4.16, the river is dominated by iron-bearing sediments, with the main component being iron hydroxide precipitate. When the pH is greater than 4.16, the river is dominated by aluminum-bearing sediments, with the main component being aluminum hydroxide precipitate. Using methods such as SEM-EDS, XRF, and XRD for mineral characterization analysis, and employing the PHREEQC software to establish a geochemical model, the main minerals of the sediments in acid mine drainage (AMD) within the study area have been further identified.

Through systematic sampling and experimental analysis of the acidic water in the Xiaomixi Stream, this study identified significant patterns in the changes of Fe and Al ions along the hydrological path of the river, and it explored the migration and transformation processes of Fe and Al ions in acidic water, as well as their influencing factors. This result contributes to providing more comprehensive theoretical support for water quality improvement and ecological restoration efforts.

4.4. Prevention and Control Strategies for Acidic Water

In response to the current pollution status of the Xiaomixi Stream in this study area, the following governance measures can be taken.

(1) The oxidation of pyrite in waste residue dumps leads to the entry of Fe ions into the water, which can be controlled at the source. Passivation treatment technology can be adopted for the pollution source. Passivation treatment technology is based on a certain reaction process, which forms an insoluble and inert coating on the mineral surface, isolating it from contact with oxidants, thereby inhibiting the oxidation of sulfur minerals and reducing Fe ions in surface water [53].

(2) The overall pH of the river is around 3–4, indicating a high acidity level. The neutralization method is the most commonly used AMD remediation technology [54]. This method involves adding a certain amount of alkaline substances, such as limestone, lime milk, and sodium hydroxide, to the wastewater, which can increase the pH value and alkalinity. The Fe and Al ions in the wastewater react with hydroxides to ultimately form insoluble hydroxide precipitates [23]. The higher the pH value of the solution, the higher the OH- concentration in the solution, which is more conducive to the formation of secondary minerals through the precipitation of iron and aluminum [55], allowing surface water to meet the national integrated wastewater discharge standard (GB 8978-1996) [56].

5. Conclusions

The systematic sampling and laboratory analysis conducted in this study revealed that the acid water pollution problem in the rivers within the study area is caused by excessive levels of Fe and Al ions in the water. The iron in the water primarily originates from the oxidation of pyrite, while the aluminum comes from the dissolution of aluminum-bearing minerals in symbiotic or associated environments. The pollution exceeds the Class II standard of the "Groundwater Quality Standard" (GB/T14848-17), posing a significant risk of surface water pollution. The experimental results indicate that as the river flows from upstream to downstream, the Fe and Al ions react with each other and form iron and aluminum deposits due to the influence of the pH values. Due to the different conditions for the existence of deposits, when the pH is less than 4.16, the river is dominated by iron deposits, resulting in acidic "yellow precipitate"; when the pH is greater than 4, the river is dominated by aluminum deposits, leading to acidic "white precipitate". The Xiaomixi Stream, as a first-order tributary of the Han River, poses a serious threat to the water quality safety of the Middle Route of the South-to-North Water Diversion Project in the Han River basin. Therefore, there is an urgent need to intensify comprehensive management efforts in the study area, with long-term and periodic monitoring and treatment required. A gradual, systematic, and economically reasonable approach should be adopted to address environmental pollution issues and ensure the perpetual flow of clean water northward.

Data Availability Statement: The data presented in this study are available on request from the corresponding authors.

References

1. Luís, A.T.; Fortes, J.C.; Santisteban, M.; Dávila, J.M.; Caraballo, M.A.; Terrones-Saeta, J.M.; Diaz-Curiel, J.; Grande, J.A. Relationships between hydrogeochemistry and diatoms in acid mine drainage affected media: The case of Iberian pyrite belt; functioning models for an all metallogenetic province. *J. Geochem. Explor.* **2024**, *264*, 107537. [CrossRef]

2. Shan, Y. Water-Rock Interaction in Coal-Bearing Strata and Environmental Effect of Coal Mine Water. Ph.D. Thesis, China University of Mining and Technology, Xuzhou, China, 2009.

3. Huang, Y.; Li, X.T.; Jiang, Z.; Liang, Z.L.; Wang, P.; Liu, Z.H.; Li, L.Z.; Yin, H.Q.; Jia, Y.; Huang, Z.S.; et al. Key factors governing microbial community in extremely acidic mine drainage (pH < 3). *Front. Microbiol.* **2021**, *12*, 761579.

4. Chandra, G.V.; Ghosh, P.K. Groundwater quality in high-sulfur coal mining region of India: Spatial distribution, source control, and health risk assessment. *J. Environ. Manag.* **2024**, *368*, 122281. [CrossRef] [PubMed]

5. Bi, D.; Yin, G. Prevention and control AMD situation and its developing trend. *J. Jiaozuo Inst. Technol. (Nat. Sci.)* **2003**, *22*, 35–38.

6. Schaider, L.A.; Senn, D.B.; Estes, E.R.; Brabander, D.J.; Shine, J.P. Sources and fates of heavy metals in a mining-impacted stream: Temporal variability and the role of iron oxides. *Sci. Total Environ.* **2014**, *490*, 456–466. [CrossRef]

7. Yuan, J.; Ding, Z.; Bi, Y.; Li, J.; Wen, S.; Bai, S. Resource utilization of acid mine drainage (AMD): A review. *Water* **2022**, *14*, 2385. [CrossRef]

8. Romero, F.M.; Canet, C.; Alfonso, P.; Zambrana, R.N.; Soto, N. The role of cassiterite controlling arsenic mobility in an abandoned stanniferous tailings impoundment at Llallagua, Bolivia. *Sci. Total Environ.* **2014**, *481*, 100–107. [CrossRef]

9. Xu, Y.; He, F.; Zhang, J. The problems of environmental geology and database formining in Northwestern China. *Northwestern Geol.* **2002**, *35*, 154–166.

10. Zhou, Y.; Short, M.D.; Li, J.; Fan, R.; Qian, G. Non-carbonate geochemical options for long-term sustainable acid and metalliferous drainage control at-source. *Environ. Earth Sci.* **2019**, *78*, 157. [CrossRef]

11. Akcil, A.; Koldas, S. Acid Mine Drainage (AMD): Causes, treatment and case studies. *J. Clean. Prod.* **2006**, *14*, 1139–1145. [CrossRef]

12. RoyChowdhury, A.; Sarkar, D.; Datta, R. Remediation of acid mine drainage-impacted water. *Curr. Pollut. Rep.* **2015**, *1*, 131–141. [CrossRef]

13. Dang, P.T.; Dang, V.C. Mine water treatment in hongai coal mines. *E3S Web Conf.* **2018**, *35*, 01007. [CrossRef]

14. Bachtlin, A. Acid mine drainage and the techniques to cleanup this issue. *DU Quark* **2019**, *3*, 28–34.

15. Zhao, L.; Wang, R.; Li, G.; Chen, M. Processing of Acid Mine Drainage and Development Prospect of Source Control Technology. *Metal Mine* **2009**, *7*, 131–135.

16. Ding, D.; Yang, S.; Zhou, W.; Xiong, Y. Treatment Method of Acid Wastewater in Opencast Coal Mine—A Case Study of Pilonghe Coal Mine in Fuquan. *Guizhou Geol.* **2022**, *39*, 400–403.

17. Simate, G.S.; Ndlovu, S. (Eds.) *Acid Mine Drainage: From Waste to Resources*; CRC Press: Boca Raton, FL, USA, 2021.

18. Acharya, B.S.; Kharel, G. Acid mine drainage from coal mining in the United States–An overview. *J. Hydrol.* **2020**, *588*, 125061. [CrossRef]

19. Bo, L. *Process and Mechanism of Alumina Minerals Inhibiting the Oxidation Dissolution of Pyrite in Acid Mine Water*; Southwest University of Science and Technology: Mianyang, China, 2023.

20. Bigham, J.M.; Nordstrom, D.K. Iron and aluminum hydroxysulfates from acid sulfate waters. *Rev. Mineral. Geochem.* **2000**, *40*, 351–403. [CrossRef]

21. Environmental Risks and Hidden Dangers in Haoping River in Ankang City, Shaanxi Province Are Outstanding, and Key Environmental Governance Work Is Slowly Progressing. China Environment Supervision 2022, 32–33. Available online: https://www.mee.gov.cn/ywgz/zysthjbhdc/dcjl/202112/t20211229_965594.shtml (accessed on 21 March 2023).

22. Tiwary, R.K. Environmental impact of coal mining on water regime and its management. *Water Air Soil Pollut.* **2001**, *132*, 185–199. [CrossRef]

23. Tong, L.; Fan, R.; Yang, S.; Li, C. Development and status of the treatment technology for acid mine drainage. *Min. Metall. Explor.* **2021**, *38*, 315–327. [CrossRef]

24. Liu, G.W.; Bai, R.C. Development of the acidic mining wastewater treatment technology. *Appl. Mech. Mater.* **2013**, *295*, 1372–1375. [CrossRef]

25. Bode'nan, F.; Baranger, P.; Piantone, P.; Lassin, A.; Azaroual, M.; Gaucher, E.; Braibant, G. Arsenic behaviour in gold-ore mill tailings, Massif Central, France: Hydrogeochemical study and investiga-tion of in situ redox signatures. *Appl. Geochem.* **2004**, *19*, 1785–1800. [CrossRef]

26. Meng, X.; Zhang, J.; Wang, Q.; Zhu, L. Analysis of Non-Point Source Pollution Characteristics of Ankang Section in the Hanjiang River Basin. *Hunan Agric. Sci.* **2023**, *10*, 35–42, 49.

27. He, J.; Li, G.; Liu, Q.; Li, L.; Chen, W.; Yu, Q. Cost Compensation Standard for Water Source Protection in Ankang Section of Hanjiang River in Middle Route of South-to-north Water Transfer Project—Based on Investigation of Ten Counties and Districts in Ankang City of Shaanxi Province. *Bull. Soil Water Conserv.* **2016**, *36*, 281–286.

28. Cui, Y.; Cui, W.; Meng, Q. Heavy Metal Pollution and Ecological Risk Assessment in the Haoping Rock Phosphate Mine Area of Shaanxi Province. *Conserv. Util. Miner. Resour.* **2021**, *41*, 157–162.

29. Jia, Z. Geological Characteristics of the Haoping Rock Phosphate Mine Belt in Ankang City. *Value Eng.* **2014**, *33*, 310–311.

30. Wu, K. Discussion on the current status of water conservancy projects in Ziyang County and the development goals of the "14th Five-Year Plan". *Ground Water* **2022**, *44*, 325–326. [CrossRef]

31. Xu, Q.; Tao, Z.; Yang, Z.; Zhang, Y. Distribution Characteristics of pH, Eh, and T in Surface Sediments from the Nantong Section of the Yangtze River. *World Nonferrous Met.* **2021**, *8*, 74–75.

32. Shi, J.; Du, P.; Luo, H.; Chen, J.; Zhang, Y.; Wu, M.; Xu, G. Characteristics and risk assessment of soil polluted by lead around various metal mines in China. *Int. J. Environ. Res. Public Health* **2021**, *18*, 4598. [CrossRef] [PubMed]

33. Saria, L.; Shimaoka, T.; Miyawaki, K. Leaching of heavy metals in acid mine drainage. *Waste Manag. Res.* **2006**, *24*, 134–140. [CrossRef] [PubMed]

34. Xu, Y.; Chen, H.; Ke, H.; Gong, H.; Cheng, X.; Zhang, M.; Wang, X.; Zhao, Z. Analysis of White Pollution of River Aluminum in Stone CoalMining Area in Haoping River Basin and Its Causes. *Northwestern Geol.* **2023**, *56*, 128–140.

35. Flores, H.; Lorenz, S.; Jackisch, R.; Tusa, L.; Contreras, I.C.; Zimmermann, R.; Gloaguen, R. UAS-based hyperspectral environmental monitoring of acid mine drainage affected waters. *Minerals* **2021**, *11*, 182. [CrossRef]

36. Lu, C.; Yang, B.; Cui, X.; Wang, S.; Qu, C.; Zhang, W.; Zhou, B. Characteristics and Environmental Re sponse of White Secondary Mineral Precipitate in the Acid Mine Drainage From Jinduicheng Mine, Shaanxi, China. *Bull. Environ. Contam. Toxicol.* **2021**, *107*, 1012–1021. [CrossRef] [PubMed]

37. Sienkiewicz, E.; Gąsiorowski, M. The evolution of a mining lake-From acidity to natural neutralization. *Sci. Total Environ.* **2016**, *557*, 343–354. [CrossRef]

38. Wu, P.; Tang, C.; Liu, C.; Zhu, L.; Pei, T.; Feng, L. Geochemical distribution and removal of As, Fe, Mn and Al in a surface water system affected by acid mine drainage at a coalfield in Southwestern China. *Environ. Geol.* **2009**, *57*, 1457–1467. [CrossRef]

39. Zhang, M.; Li, W.; Wang, P.; Wei, X.; Zhu, J.; Liu, S. Study on Generation mechanism of acid drainage from a waste stone coal mine in Ziyang, Shaanxi Province. *China Energy Environ. Prot.* **2024**, *46*, 245–250.

40. Sun, Y.; Dong, J.; Wang, X. Research on Inverting Models of Aboveground Biomass in Typical Grasslands of Xilin Gol League Based on ASD Field Spectroradiometer. *Acta Agrestia Sin.* **2024**, *32*, 2234–2244.

41. Šubrt, J.; Michalková, E.; Boháček, J.; Lukáč, J.; Gánovská, Z.; Máša, B. Uniform particles formed by hydrolysis of acid mine drainage with urea. *Hydrometallurgy* **2011**, *106*, 12–18. [CrossRef]

42. Xue, S.; Ke, W.; Zeng, J.; Tabelin, C.B.; Xie, Y.; Tang, L.; Xiang, C.; Jiang, J. Pollution prediction for heavy metals in soil-groundwater systems at smelting sites. *Chem. Eng. J.* **2023**, *473*, 145499. [CrossRef]

43. Tang, L.; Gao, W.; Lu, Y.; Tabelin, C.B.; Liu, J.; Li, H.; Yang, W.; Tang, C.; Feng, X.; Jiang, J.; et al. The formation of multi-metal (loid) s contaminated groundwater at smelting site: Critical role of natural colloids. *J. Hazard. Mater.* **2024**, *471*, 134408. [CrossRef] [PubMed]

44. Basallote, M.D.; Cánovas, C.R.; Olias, M.; Pérez-López, R.; Macías, F.; Carrero, S.; Ayora, C.; Nieto, J.M. Mineralogically-Induced Metal Partitioning during the Evaporative Precipitation of Efflorescent Sulfate Salts from Acid Mine Drainage. *Chem. Geol.* **2019**, *530*, 119–339. [CrossRef]

45. Lee, J.S.; Chon, H.T. Hydrgeochemical characteristics of acid mine drainage in the vicinity of an abandoned mine, Daduk Creek, Korea. *J. Geochem. Explor.* **2006**, *88*, 37–40. [CrossRef]

46. Carrero, S.; Pérez-López, R.; Fernandez-Martinez, A.; Cruz-Hernández, P.; Ayora, C. Poulain The potential role of aluminium hydroxysulphates in the removal of contaminants in acid mine drainage. *Chem. Geol.* **2015**, *417*, 414–423. [CrossRef]

47. Miner, D.K. Nordstrom. Effects of microbiological and geochemical interactions in mine drainage. *Assoc. Can. Short. Course* **2003**, *31*, 227.

48. España, J.S.; Pamo, E.L.; Pastor, E.S.; Andrés, J.R.; Rubí, J.M. The Removal of Dissolved Metals by Hydroxysulphate Precipitates during Oxidation and Neutralization of Acid Mine Waters, Iberian Pyrite Belt. *Martín Rubí. Aquat. Geochem.* **2006**, *12*, 269–298. [CrossRef]

49. Espana, J.S.; Pamo, E.L.; Santofimia, E.; Aduvire, O.; Reyes, J.; Barettino, D. Acid mine drainage in the Iberian Pyrite Belt (Odiel river watershed, Huelva, SW Spain): Geochemistry, mineralogy and environmental implications. *Barettino. Appl. Geochem.* **2005**, *20*, 1320–1356. [CrossRef]

50. Van Wyk, N. Investigation into the Sustainable Use of Mine Waste to Treat or Prevent Acid Mine Drainage. Ph.D. Thesis, North-West University, Potchefstroom, South Africa, 2023.

51. Pacella, A.; Tomatis, M.; Viti, C.; Bloise, A.; Arrizza, L.; Ballirano, P.; Turci, F. Thermal inertization of amphibole asbestos modulates Fe topochemistry and surface reactivity. *J. Hazard. Mater.* **2020**, *398*, 123119. [CrossRef]

52. España, J.S. The behavior of iron and aluminum in acid mine drainage: Speciation, mineralogy, and environmental significance. In *Thermodynamics, Solubility and Environmental Issues*; Elsevier: Amsterdam, The Netherlands, 2007; pp. 137–150.

53. Ji, M.K.; Yoon, H.S.; Ji, E.D.; Lee, W.R.; Park, Y.T.; Yang, J.S.; Jeon, B.H.; Shim, Y.S.; Kang, M.H.; Choi, J.Y. Development of control technology for acid mine drainage by coating on the surface of pyrite using chemicals. *J. Soil Groundw. Environ.* **2010**, *15*, 46–52.

54. Tolonen, E.T.; Sarpola, A.; Hu, T.; Rämö, J.; Lassi, U. Acid mine drainage treatment using by-products from quicklime manufacturing as neutralization chemicals. *Chemosphere* **2014**, *117*, 419–424. [CrossRef] [PubMed]

55. Wang, Z. Experimental simulation of mine water acidification under the action of pyrite. Master's Thesis, Henan University of Science and Technology, Jiaozuo, China, 2023. [CrossRef]

56. Pohl, A. Removal of heavy metal ions from water and wastewaters by sulfur-containing precipitation agents. *Water Air Soil Pollut.* **2020**, *231*, 503. [CrossRef]